Remote Sensing Applications: Society and Environment 40 (2025) 101802

Contents lists available at ScienceDirect

Remote Sensing Applications: Society and Environment

journal homepage: www.elsevier.com/locate/rsase

Analysis of hyperspectral data to define multispectral sensor specifications for enhancing plastic greenhouse detection

Francesca Despini [a], Sofia Costanzini [b], Davide Parmeggiani [a], Daniele la Cecilia [c,*]

[a] Department of Engineering Enzo Ferrari, University of Modena and Reggio Emilia, Italy
[b] Green Office, Technical Building, Facility management and sustainability, University of Modena and Reggio Emilia, Italy
[c] Department of Civil, Environmental and Architectural Engineering, University of Padua, Italy

ARTICLE INFO

Keywords:
Protected agriculture
Remote sensing
Spectral indices
Hyperspectral
Land cover classification

ABSTRACT

Sentinel-2 and Landsat-9 multispectral operational missions enable global and continuous land-cover classification. These missions have been increasingly used to map plastic greenhouses; however, several misclassification issues were reported due to spectral similarities with other land covers. This research uses airborne hyperspectral data to demonstrate that plastic greenhouses can be reasonably mapped upon acquiring two reflectance values (ρ) in the Short-Wave InfraRed (SWIR) spectrum, at $\rho_{max} = 1644$ nm and $\rho_{min} = 1729$ nm, or alternatively at $\rho_{max} = 2130$ nm and $\rho_{min} = 2315$ nm. Consequently, we developed a Normalized Difference Greenhouse Index, NDGI $= \frac{\rho_{max}-\rho_{min}}{\rho_{max}+\rho_{min}}$, for each alternative selection. These new indices rely on the spectral slope between characteristic wavelengths in the SWIR region rather than on the absolute depth of the absorption feature as a possible improvement to the unexplored Hydrocarbon Index (HI). The NDGI classified plastic greenhouses in a heterogeneous landscape with an accuracy of 93 % using high-resolution data. Still, calculating the NDGI with PRISMA (*PRecursore IperSpettrale della Missione Applicativa*) imagery revealed the method's transferability to coarser spatial resolutions despite a reduced separability inherently emerged. Furthermore, PRISMA data revealed that incorporating the bands for the NDGI would substantially reduce the number of false positives when using the Sentinel-2 based Open field and Protected Agriculture Classifier in the presence of critical highly reflective land covers. This study indicates that NDGI will enable efficient, fast, and operational mapping of plastic greenhouses globally through current hyperspectral missions (e.g., PRISMA by ASI, EnMAP by DLR, HISUI by JAXA, and Tanager by Planet) including the upcoming ones (e.g., NASA's Surface Biology and Geology mission – SBG and ESA's CHIME). Likewise, upgraded multispectral missions such as Landsat Next and Sentinel-2 Next Generation (NG) could integrate the identified spectral bands and allow for operational monitoring of plastic greenhouses.

1. Introduction

The expansion of plastic greenhouses has provided numerous benefits in protected agriculture (Wittwer, 1993), resulting from the realization of controlled environments and extended growing seasons (Giacomelli and Roberts, 1993; Savic and Ilin, 2022; Robson

* Corresponding author. Department of Civil, Environmental and Architectural Engineering University of Padua 35131 Padua, Italy.
E-mail address: daniele.lacecilia@unipd.it (D. la Cecilia).

https://doi.org/10.1016/j.rsase.2025.101802
Received 17 July 2025; Received in revised form 14 November 2025; Accepted 17 November 2025
Available online 20 November 2025

et al., 2022). These structures contribute to efficiently increase crops' yield, reduce water usage, and improve crop protection from pests and extreme weather conditions (Espí et al., 2006; Ahemd et al., 2016; Yang et al., 2017; Hu et al., 2021; Briassoulis, 2023). Protected agriculture represents a strategic response to the growing demand for sustainable food production under increasing demographic and environmental pressures (Aznar-Sánchez et al., 2020). Plastic greenhouses are sprawling globally, particularly in rural areas and low-income countries, thanks to their economicity in relation to the boost in agricultural production.

The widespread use of plastic greenhouses also presents significant environmental challenges from multiple perspectives. The plastic waste mismanagement and degradation of plastic materials during the cropping cycle would lead to the accumulation of plastic debris in agricultural fields and in the environment, which can persist for decades and contribute to soil and water contamination (Wang et al., 2022; Qi et al., 2023). These issues can negatively impact soil health, local ecosystems, and biodiversity (Chen et al., 2022; Tang, 2023). Plastic residues can interfere with soil structure, water infiltration, and microbial activity, ultimately reducing soil fertility and crop productivity (Wang et al., 2016). Additionally, leaching of plastic additives and microplastics into the environment poses risks to aquatic ecosystems and human health, as these contaminants can enter the food chain through water runoff and crop uptake (Lehel and Murphy, 2021; Guo et al., 2020; Huang et al., 2020). Given these environmental concerns, it is crucial to accurately map and timely monitor plastic greenhouses for a better understanding of their distribution and impact.

Remote sensing technology offers a powerful tool for mapping plastic greenhouses and it is being increasingly exploited for this purpose (Veettil et al., 2023; Aguilar et al., 2021; Jiménez-Lao et al., 2020). A plethora of satellites and computational approaches have been used to map plastic greenhouses. These span over fast and simple index-based classification of pixels based on multi-spectral data, such as the Advanced Plastic Greenhouse Index (APGI by Zhang et al., 2022), increasingly complex machine learning classification models (Aguilar et al., 2020, 2021; Lanorte et al., 2017; Acharki et al., 2024), up to artificial intelligence models pre-trained to detect and classify greenhouse structures from high spatial resolution natural color imagery (Tong et al., 2024). Each approach has its advantages and disadvantages.

The classification speed of indices and pixel-based models built using multi-spectral information is challenged by loss in accuracy due to the spectral similarities with other land cover types, such as bare soil, urban areas, and other reflective surfaces (Jiménez-Lao et al., 2022; Aguilar et al., 2020; Shi et al., 2019, la Cecilia et al., 2023). While the classification outcome can be improved through exclusion masks (la Cecilia and Despini, 2025) or processing methodologies like pan-sharpening (Jiménez-Lao et al., 2020), it remains challenging to achieve consistent classifications across different contexts. On another side, artificial intelligence models for image recognition (Tong et al., 2024) are robust, but are computationally demanding, time consuming, and necessitates costly data. Moreover, machine learning and artificial intelligence techniques have not yet been systematically explored for sub-pixel classification, which could help address the mixed-pixel problem that often limits greenhouse mapping accuracy.

Hyperspectral satellite data unlock unparalleled capabilities for detecting plastic materials as they capture a much broader electromagnetic spectrum at closer intervals, providing detailed spectral information that can be used to identify different materials (McCullum et al., 2021). However, hyperspectral data also come with larger data volumes and more complex data processing requirements (Vali et al., 2020; Hati et al., 2021). Zhou et al. (2022) test hyperspectral data for mapping plastic greenhouses acquired with the Chinese satellite GAOFEN-5 and the Italian PRISMA. More recently, NASA's EMIT imaging spectrometer has been used to perform the first global detection of plastics (HDPE and PVC) at 60 m spatial resolution (Estrela et al., 2024). This represents a major step forward in demonstrating the feasibility of global plastic monitoring from spaceborne imaging spectroscopy. However, each of the aforementioned satellite dataset has its own constrain spanning from the limited data accessibility, acquisition of images on demand, the relatively coarse spatial resolution, or the limited orbital coverage in the case of the ISS. A relevant index for detecting plastics using airborne hyperspectral data was the Hydrocarbon Index (HI by Kühn et al., 2004 and Garaba and Dierssen, 2018). The index was originally developed for the detection of hydrocarbons and marine plastics using shortwave infrared (SWIR) absorption features in two formulations. The first formulation (Kühn et al., 2004) exploits three adjacent bands around 1705, 1729, and 1741 nm, corresponding to the strong absorption near 1732 nm. The second formulation (Garaba and Dierssen, 2018) uses three bands around 1197, 1216, and 1235 nm, targeting the absorption feature near 1215 nm.

Our study systematically tests hyperspectral data and identifies the most relevant absorption features for plastic greenhouse detection and demonstrates how they can be operationalized into two novel simplified indices (i.e., $NDGI_i$). The results provide a clear indication of which spectral bands contain the necessary information if selected from hyperspectral missions or incorporated into future multispectral satellite designs for enabling continuous, large-scale, and cost-effective monitoring of plastic greenhouses worldwide. Our study includes an assessment on the importance of spatial and spectral resolution of hyperspectral data by comparing airborne data and satellite data. Finally, we used original PRISMA data to test the interoperability of the algorithm between the airborne AVIRIS-NG and the spaceborne PRISMA sensors over the *Piana del Sele* area, while PRISMA imagery was used for other study sites relevant to greenhouse mapping.

In perspective, the operational use of this methodology could support public agencies in maintaining accurate and up-to-date information on the distribution of plastic greenhouses. It may also provide valuable input for other scientific domains: for example, consistent maps of plastic greenhouses can improve the impact assessment on meteorology (Campra and Millstein, 2013 – showing a reduction in air temperatures) and hydrology (la Cecilia et al., 2025b – offering the possibility to update the modelling and parametrization of processes).

2. Methods and datasets

2.1. Study areas and remote sensing data availability

Five study areas were chosen for investigating the hyperspectral signatures of plastic greenhouses and other agricultural land covers. Four areas were located in Europe and one area in China as shown in Fig. 1. High-spatial (2.7 m) resolution airborne hyperspectral imagery was available for one area (i.e., *Piana del Sele*, Italy), while spaceborne hyperspectral imagery at 30 m resolution was available for the same area and for the other study areas as detailed in Table 1. The high spatial resolution (2.7 m) imagery in *Piana del Sele* was necessary for a detailed investigation of the hyperspectral signatures of plastic greenhouses, which may have sizes smaller than 30 m in width. This area was used to formulate a robust index for plastic greenhouse mapping as well as assess the possibility to maintain the information of pixels with 2.7 m resolution to those at 30 m. The *Piana del Sele* area was selected also for the direct knowledge of the site by the authors. Several field visits provided ground-truth information, used for the validation of the remote sensing analyses. Other two areas were chosen in the Netherlands and China. The interest there was to test the robustness of the classification index for glass-covered greenhouses in the first case, and in the country with the highest area of plastic greenhouses, in the second case. The last two areas were chosen in Turkey and Poland. There, the random forest-based Open field and Protected Agriculture Classifier (OPAC) (la Cecilia et al., 2023), developed for multi-spectral Sentinel-2 data, created a high number of false positives at the pixel level. These areas were characterized, respectively, by highly reflective bare soils and highly reflective built-up structures within farmlands (la Cecilia and Despini, 2025). The novel classification index proposed in this study was expected to have the capability to distinguish between greenhouse roofs made of plastic materials and other non-agricultural structures. We anticipate that the robustness of the NDGI was demonstrated using the AVIRIS-NG dataset over *Piana del Sele*, while its transferability to spaceborne conditions was evaluated using PRISMA data. In this study, we focused on polyethylene (PE), the most widely used polymer for greenhouse coverings, as the reference material for our analysis (Scarascia-Mugnozza et al., 2011; Hussain and Hamid, 2003).

2.2. Hyperspectral data evaluation and analysis

This study used airborne and spaceborne hyperspectral data to identify the most effective spectral bands in the Visible - Near InfraRed (VNIR) and Short-Wave InfraRed (SWIR) regions to effectively and parsimoniously distinguish plastic greenhouses from other land covers.

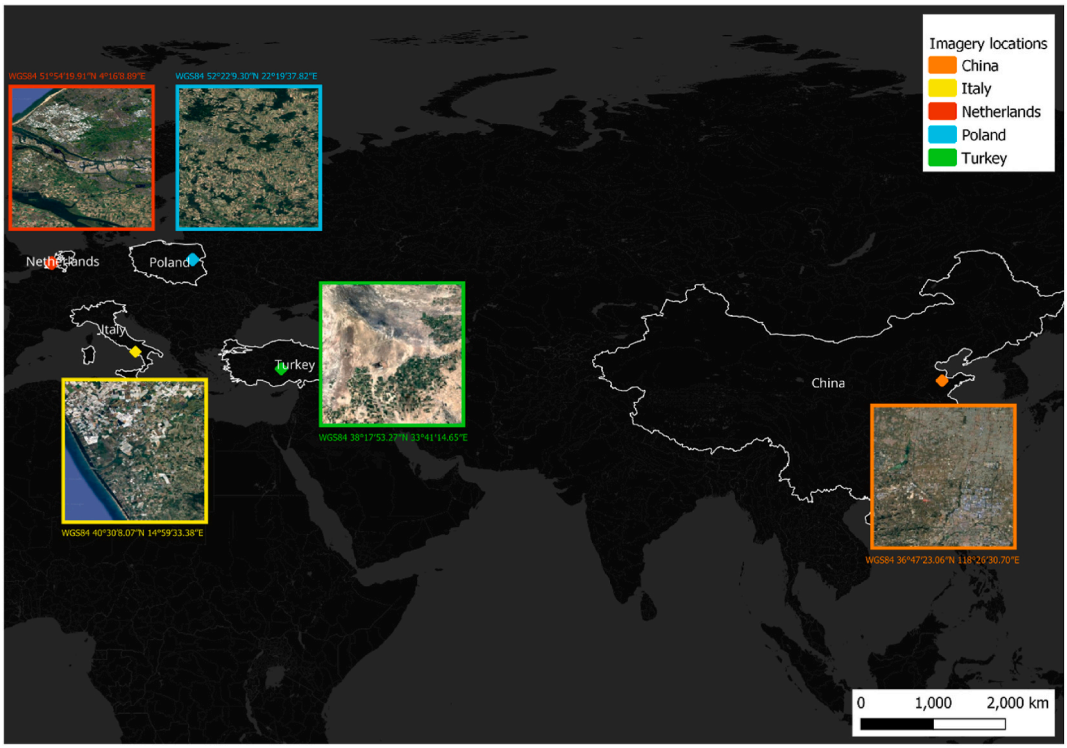

Fig. 1. Global view of the study areas.

Table 1
Overview of chosen study areas where hyperspectral images were acquired to evaluate the robustness and transferability of greenhouse classification indices under varying environmental and structural conditions. Coordinates are reported as scene centers in decimal degrees. Detailed scene information, including Scene IDs and geographic bounding boxes, is provided in Supplementary Table S1.

Country	Scene Center (Decimal Degrees)	Sensor	Acquisition time (dd/mm/yyyy)	Description
Italy	40.5022° N 14.9926° E	AVIRIS-NG (2.7 m resolution)	June 03, 2021	The majority of the greenhouses in *Piana del Sele* are multi-tunnels in polyethylene, used to produce some cut leafy vegetables ready-to-eat (la Cecilia et al., 2025b; Picariello et al., 2024).
Italy	40.5405° N 14.9717° E	PRISMA (30 m resolution)	May 11, 2021	The majority of the greenhouses in *Piana del Sele* are multi-tunnels in polyethylene, used to produce some cut leafy vegetables ready-to-eat (la Cecilia et al., 2025b; Picariello et al., 2024).
China	36.7897° N 118.4419° E	PRISMA (30 m resolution)	April 21, 2020	This region is characterized by a high density of plastic greenhouses, primarily used for intensive agricultural production. The spectral signatures of these structures may vary due to different roofing materials and colours, possibly decreasing the classification accuracy (Liu et al., 2019; Liu and Xin, 2023; Tong et al., 2024).
The Netherlands	51.9055° N 4.2691° E	PRISMA (30 m resolution)	March 22, 2020	The Netherlands is known for its extensive glass greenhouses, which result in different spectral properties (Gerritsen et al., 2014; De Gelder et al., 2011).
Turkey	38.2981° N 33.6874° E	PRISMA (30 m resolution)	April 30, 2021	This area features highly reflective soils rich in carbonate calcium, which can cause spectral confusion between greenhouses and natural surfaces (Kendirli, 2006).
Poland	52.3693° N 22.3272° E	PRISMA (30 m resolution)	September 03, 2024	In Poland, it was found that many agricultural structures (i.e., highly reflective roofs of farmyards) were misclassified as greenhouses (Kuśmierski and Hodor, 2024).

2.2.1. AVIRIS-NG imagery for extracting hyperspectral signatures and formulating a robust plastic greenhouse classification index

For the purposes of analyzing the spectrum of greenhouses and other target land covers as well as tentatively identify specific absorption features in the spectrum of plastic materials, with the necessary spatial and spectral accuracy, we resorted to airborne hyperspectral data. Airborne hyperspectral images enable the processing of data with a quality level comparable to laboratory analyses (Levin et al., 2007; Zhou et al., 2022). In particular, we retrieved an image acquired in the Airborne Visible/InfraRed Imaging Spectrometer - Next Generation (AVIRIS-NG) mission over *Piana del Sele*, an area with an important plastic greenhouse district (la Cecilia et al., 2025b), making it an ideal site for investigating plastic greenhouse detection using remote sensing technologies. This AVIRIS-NG acquisition was part of the 2021's joint effort between the European Space Agency (ESA) with the Copernicus

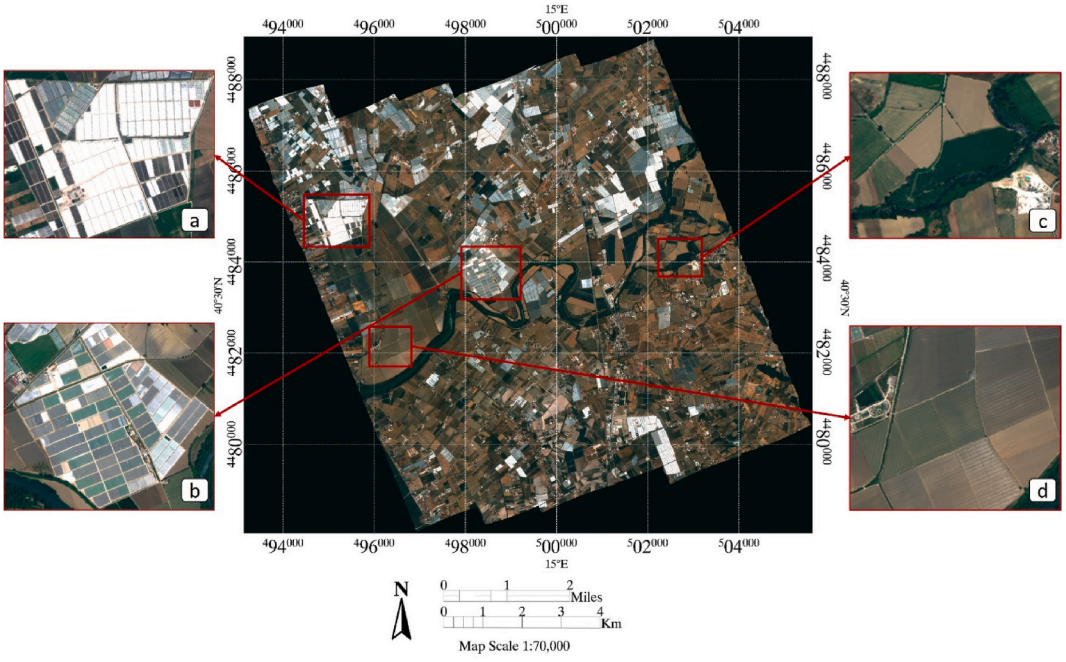

Fig. 2. AVIRIS image of the Piana del Sele area. True color composition. The red boxes highlight examples of the four selected Regions of Interest (ROIs): a) white greenhouses, b) transparent plastic greenhouses, c) vegetation, and d) bare soil. Center scene coordinates: WGS84 40.5022° N and 14.9926° E.

Hyperspectral Imaging Mission for the Environment (CHIME) and the Jet Propulsion Laboratory (JPL) together with the University of Zurich with the Surface Biology and Geology (SBG) mission. The objective of the campaign was to collect high-quality hyperspectral data over European sites in order to support calibration and validation activities, and to test potential applications of future spaceborne missions in agriculture, ecosystem monitoring, and geology. Both CHIME and SBG are forthcoming satellite missions that aim to advance the use of hyperspectral imaging for environmental monitoring and geological applications; in 2021, their objectives were simulated through the airborne AVIRIS-NG campaign. AVIRIS-NG represents a significant advancement over the classic AVIRIS sensor, offering finer spectral resolution (5 nm compared to 10 nm), improved signal-to-noise ratio, and enhanced radiometric stability, while covering a similar spectral range (380–2510 nm) (Chapman et al., 2019; Thorpe et al., 2016; Green et al., 1998).

The image over *Piana del Sele* was taken on June 3, 2021, and covered an area of about 136 km^2 (Fig. 2). The scene spans from Upper Left (UL) corner at WGS84 40.5513° N, 14.9190° E to Lower Right (LR) corner at 40.4531° N, 15.0661° E, covering the entire agricultural district. Although a 1-m spatial resolution image was available, a 2.7-m resolution was chosen for computational efficiency. This resolution was deemed more than adequate for the study's objectives. The AVIRIS-NG dataset was downloaded as Level-2 surface reflectance data from the JPL/AVIRIS data portal (Green et al., 2023), already corrected for atmospheric and radiometric distortions using the standard ATREM/FLAASH chain (Thompson et al., 2015; Green et al., 1998). While these corrections

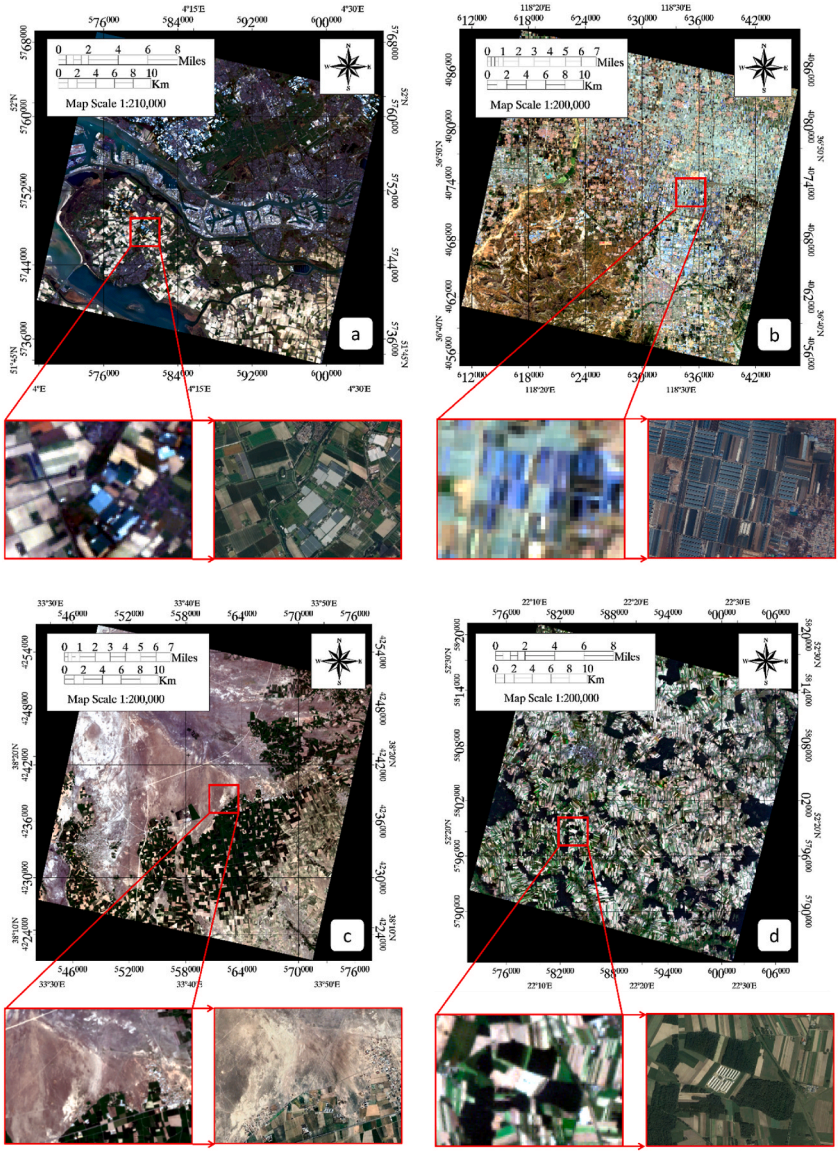

Fig. 3. PRISMA true color images of four study areas: (a) the Netherlands, (b) China, (c) Turkey, and (d) Poland. Red boxes highlight regions identified as critical for classification due to spectral confusion or mislabelling. Specifically: (a) glass greenhouses, (b) typical Chinese greenhouse structures, (c) bare soils, and (d) agricultural areas misclassified as greenhouses. The nature of these areas (sometimes actual greenhouses, sometimes not) was visually verified using high-resolution Google Earth imagery and expert knowledge of the sites.

substantially reduce atmospheric and radiometric distortions, we acknowledge that no correction is perfect, and small-scale atmospheric variability within the study area may still introduce uncertainties in the retrieved spectra. The image consists of 425 spectral bands, covering a continuous spectrum from 377 to 2500 nm. For our analysis, we excluded bands in the ranges 1350–1450 nm and 1800–1950 nm, which are outside the main atmospheric transmission windows and are strongly affected by water vapor absorption.

Four land cover classes were considered:

- Bare soils
- Vegetation
- White greenhouses
- Transparent plastic greenhouses

ROIs for each class were delineated based on visual interpretation of the AVIRIS-NG image, supported by field knowledge and direct visits to the study area. The ROIs were distributed across the entire AVIRIS-NG image in order to capture the variability of each land cover class, and not only in the specific locations displayed in Fig. 2 (the complete set of ROIs is provided as a vector file in the supplementary material). ROIs were intentionally kept small and placed over spectrally homogeneous targets in order to minimize the influence of mixed pixels and ensure the representativeness of the extracted spectra. For each class, we also computed descriptive statistics of the spectral values (median, average, and standard deviation) to assess the internal variability of the ROIs and to exclude possible outliers. In total, 3941 pixels were selected for bare soils, 4106 for vegetation, 4131 for white greenhouses, and 3845 for transparent greenhouses. These ROIs served as ground truth for constructing average spectral profiles of each class. In particular, we visually searched for characteristic absorption features of plastic covering for developing a Normalized Difference Greenhouse Index (NDGI) to enhance the discrimination of plastic greenhouses from other surface types. The NDGI was formulated using the general expression:

$$NDGI = \frac{\rho_{max} - \rho_{min}}{\rho_{max} + \rho_{min}} \in [-1; 1]$$

Where $\rho_{\max}$ and $\rho_{\min}$ represent the local maximum and minimum, respectively, reflectance values associated with plastic-related absorption features. The index ranges from -1 to 1, with higher values indicating the likely presence of greenhouse structures.

2.2.2. *PRISMA imagery for spaceborne hyperspectral data*

PRISMA (PRecursore IperSpettrale della Missione Applicativa) is the Italian Space Agency's hyperspectral mission, launched in March 2019, designed to provide high-quality VNIR–SWIR data for applications in environmental monitoring, agriculture, and natural resource management (Loizzo et al., 2018; Pignatti et al., 2013). PRISMA is an imaging spectrometer that operates over a nominal spectral range of 400–2500 nm, utilizing two distinct instruments (Cogliati et al., 2021). The VNIR spectrometer acquires 66 spectral bands spanning approximately 400–1010 nm, with a nominal spectral sampling interval below 11 nm and a spectral bandwidth narrower than 15 nm. The SWIR detector covers the 920–2500 nm range, providing 174 spectral bands, each with a bandwidth of less than 15 nm. PRISMA features a spatial resolution of 30 m in the VNIR-SWIR spectral range and also includes a panchromatic band with a spatial resolution of 5 m.

The PRISMA images used in this study (see Scene IDs in Supplementary Table S1) were downloaded as Level 2D surface reflectance products from the ASI PRISMA user portal. These products involve bottom-of-atmosphere (BOA) reflectance (MODTRAN-based

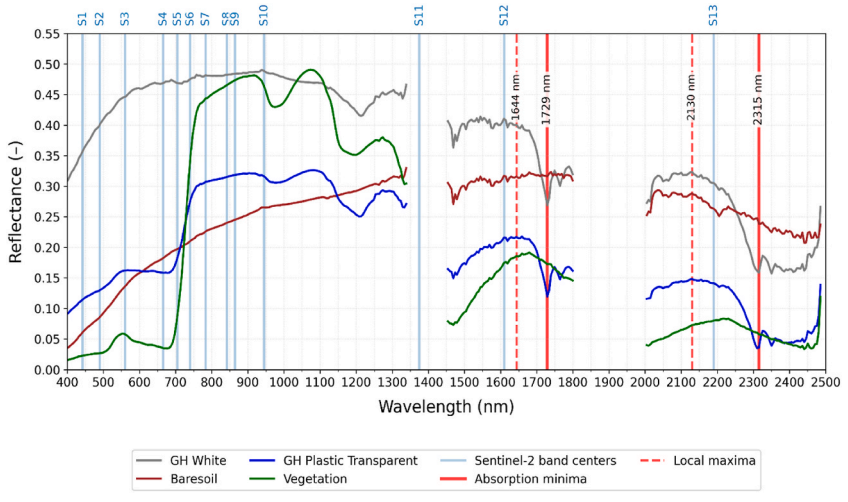

Fig. 4. Spectral signatures extracted from AVIRIS-NG imagery for the four selected ROIs. Red bands indicate plastic-related absorption features; light blue bands correspond to Sentinel-2 wavelengths.

atmospheric correction processor v.02.05), ortho-projected and geocoded (Loizzo et al., 2018; De Luca et al., 2025). Image processing was conducted in ENVI 5.2 (Harris Geospatial Solutions), with ROI selection supported by high-resolution reference imagery, and spectral analysis was further refined using Python custom scripts.

2.2.3. *Transferability of airborne hyperspectral data to spaceborne ones*

The availability of free spaceborne hyperspectral data at 30 m spatial resolution from the PRISMA mission motivated us to test whether knowledge gained from hyperspectral data with 2.7 m resolution could be transferred to data with 30 m resolution. Although six PRISMA images of the *Piana del Sele* area were available in the archive, most were affected by extensive cloud cover or did not fully capture the target agricultural area. One image was suitable in terms of spatial coverage but was acquired on a different date than the AVIRIS-NG flight. Using images acquired at different times could introduce uncertainties related to seasonal changes or short-term variations in greenhouse coverage, which would confound the comparison. To ensure that both datasets represented exactly the same conditions (weather, illumination, crop stage, and greenhouse materials), we chose to simulate a PRISMA-like image from the AVIRIS-NG dataset by averaging subsets of AVIRIS-NG bands corresponding to the central wavelengths of PRISMA bands. To achieve this, we used the "Spectral Resampling" tool in ENVI 5.2, which allows resampling to a user-defined spectral response function or to averaged bins. Specifically, for each PRISMA channel, all AVIRIS-NG bands within its nominal bandwidth were averaged, resulting in broader bandwidths (~15 nm) and reduced spectral resolution. We also tested simple band selection (choosing only the closest central wavelength), but this resulted in noisier spectra and lower separability, while averaging ensured smoother and more representative spectral profiles. Nevertheless, we analysed the available PRISMA image over *Piana del Sele* to verify that the characteristic absorption features detected in the PRISMA-like image were present in the real PRISMA data as well. The same ROIs from AVIRIS-NG were used for PRISMA, and average spectra were extracted.

Airborne data were not available for analyzing the spectrum of land cover types in the other four study areas shown in Fig. 1 and listed in Table 1, which created false positives in the classification of greenhouses with OPAC (a multispectral-based land cover classifier) (la Cecilia et al., 2023) over Europe (la Cecilia and Despini, 2025) (i.e., red boxes in Fig. 3). We visually validated these misclassifications using high-resolution Google Earth imagery and expert knowledge of the selected sites. For instance, in the Netherlands (Fig. 3a), glass greenhouses often resemble industrial or urban features. In the Chinese case (Fig. 3b), dense and possibly spectrally diverse greenhouse structures may challenge standard classification approaches. In Turkey (Fig. 3c), there exist highly reflective bright soils that resemble the white-painted plastic greenhouse in Mediterranean areas, while in Poland (Fig. 3d), certain agricultural areas were incorrectly labelled as greenhouses. These case studies exemplify the types of misclassification that arise from

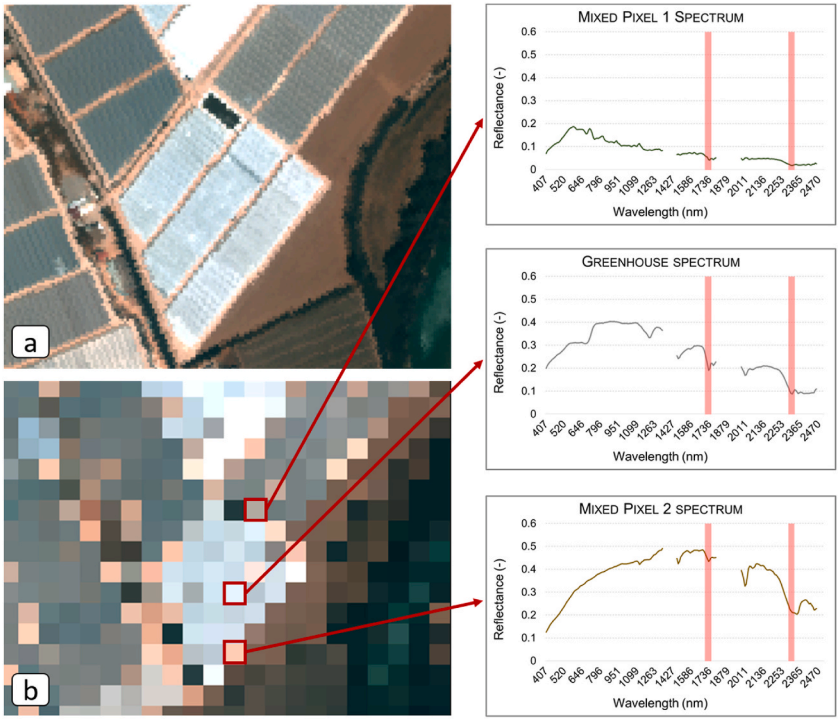

Fig. 5. Effect of spatial downsampling from 2.7 m (AVIRIS-NG) to 30 m (PRISMA-like) on the spectral signatures of greenhouse pixels. (a) True-color AVIRIS-NG image showing plastic greenhouse structures. (b) The same area after spatial aggregation to 30 m resolution, highlighting the formation of mixed pixels along greenhouse boundaries. Spectral profiles on the right show: a pure greenhouse pixel, and two neighbouring mixed pixels combining greenhouse, bare soil, and vegetation components. The absorption features at 1729 nm and 2315 nm are preserved in the pure greenhouse pixel but are attenuated in the mixed pixels due to spectral dilution.

multispectral data. Thus, we analysed the available spaceborne hyperspectral imagery from PRISMA to understand whether hyperspectral data could resolve spectral ambiguities.

3. Results

3.1. AVIRIS-NG imagery for extracting spectral signatures and developing the NDGI

The average spectra for the four selected ROIs were extracted from the AVIRIS-NG image, and they are shown in Fig. 4. The two red vertical bands indicate two clearly distinguishable absorption peaks between plastic greenhouses and other land cover types identified around 1729 nm and 2315 nm, respectively. The finding is consistent with those reported by Levin et al. (2007) and Zhou et al. (2022), who use different sensors. A third absorption peak is highlighted in the literature around 1218 nm (Kühn et al., 2004). This peak was also present in the "Vegetation" class, and therefore, was deemed unusable in this context. While hyperspectral studies specifically focused on greenhouse plastics are limited in the literature, there is a broader body of work on the use of hyperspectral imaging for the study and identification of up to twenty types of plastics in soil and water matrices (Castagna et al., 2023; Freitas et al., 2021, la Cecilia et al., 2024). All this literature corroborates the robustness of the found spectral absorption features for plastic greenhouses. The blue bands in Fig. 4 represent the central wavelengths of the Sentinel-2 multispectral sensor bands. It is evident that the Sentinel-2 bands do not align with the specific absorption features of plastic-covered greenhouses. This spectral mismatch limits the ability of multispectral data to reliably discriminate greenhouses, especially those with transparent plastic covers, from spectrally similar surfaces such as bare soil or certain types of vegetation.

According to the observed absorption peaks, two separate indices were constructed. The general form of the $NDGI_i$ was computed as:

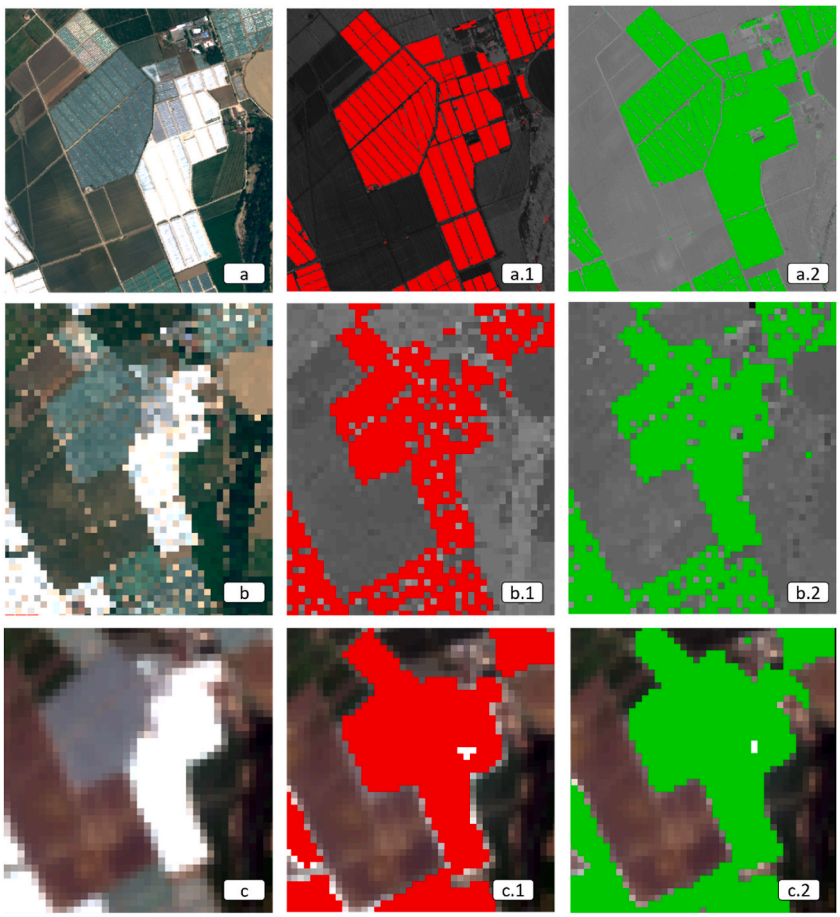

Fig. 6. Subset of the AVIRIS-NG image (a, acquired on June 03, 2021), with classification results obtained using $NDGI_1$ (a.1) and $NDGI_2$ (a.2). The same subset after PRISMA-like resampling of the AVIRIS-NG image (b), with corresponding $NDGI_1$ (b.1) and $NDGI_2$ (b.2) classifications. Panels (c), (c.1), and (c.2) show the same area from an original PRISMA image (acquired on May 11, 2021), together with $NDGI_1$ and $NDGI_2$ classification outputs. Red pixels represent greenhouse detections using $NDGI_1$, while green pixels indicate detections using $NDGI_2$. Subset coordinates: ULC: WGS84 40.5909°N, 15.0160°E; LRC:40.5198°N, 15.0298°E.

$$\mathrm{NDGI}_i = \frac{\rho_{\max_i} - \rho_{\min_i}}{\rho_{\max_i} + \rho_{\min_i}} \in [-1; 1]$$

Where the subscript *i* refers to each of the two different peaks. For the first absorption peak ($i = 1$), the local maximum reflectance ρ_{max1} was found at 1644 nm and the local minimum reflectance ρ_{min1} was at 1729 nm. For the second absorption peak ($i = 2$), the local maximum reflectance ρ_{max2} was found at 2130 nm and the local minimum reflectance ρ_{min2} was at 2315 nm. In Fig. 4, the diagnostic absorption features are highlighted (minima at 1729 nm and 2315 nm, with adjacent local maxima at 1644 nm and 2130 nm) together with the Sentinel-2 band centers to make the spectral mismatch evident.

3.2. Image simulation

Downsampling of the AVIRIS-NG image from 2.7 m to 30 m resolution highlighted the expected loss of detail in the shapes and boundaries of greenhouse structures (Fig. 5). This difference is particularly relevant when small or narrow features are under investigation, as they may be partially or completely lost due to pixel aggregation, resulting in the well-known mixed-pixel problem (Hsieh et al., 2001; la Cecilia et al., 2023).

In the simulation of PRISMA data, at least two AVIRIS-NG bands contributed to each PRISMA-like band. This band aggregation preserved the overall spectral shape while reducing the spectral resolution to match that of PRISMA, enabling a consistent comparison between the two datasets. As shown in Fig. 5, the absorption peaks remained detectable in the PRISMA-like spectra, indicating that the main spectral characteristics of greenhouse coverings are preserved. However, while the absorption features are clearly visible in the spectrum of the pure greenhouse pixel, they appear attenuated or partially masked in the neighbouring mixed pixels due to spectral averaging with the surrounding land covers. This illustrates the typical spectral dilution effect introduced by coarse spatial resolution, which can reduce the separability of narrow or spatially confined targets.

The identification of pure and mixed pixels was based on visual interpretation of very high-resolution reference imagery (Google Earth and field surveys), which allowed confirming the presence and shape of individual greenhouse structures within each pixel footprint. The spectral signatures of mixed pixels qualitatively resembled the linear combination of neighbouring endmembers (greenhouses, soil, and vegetation), consistently with the expected behaviour of a linear spectral mixing model (Hsieh et al., 2001).

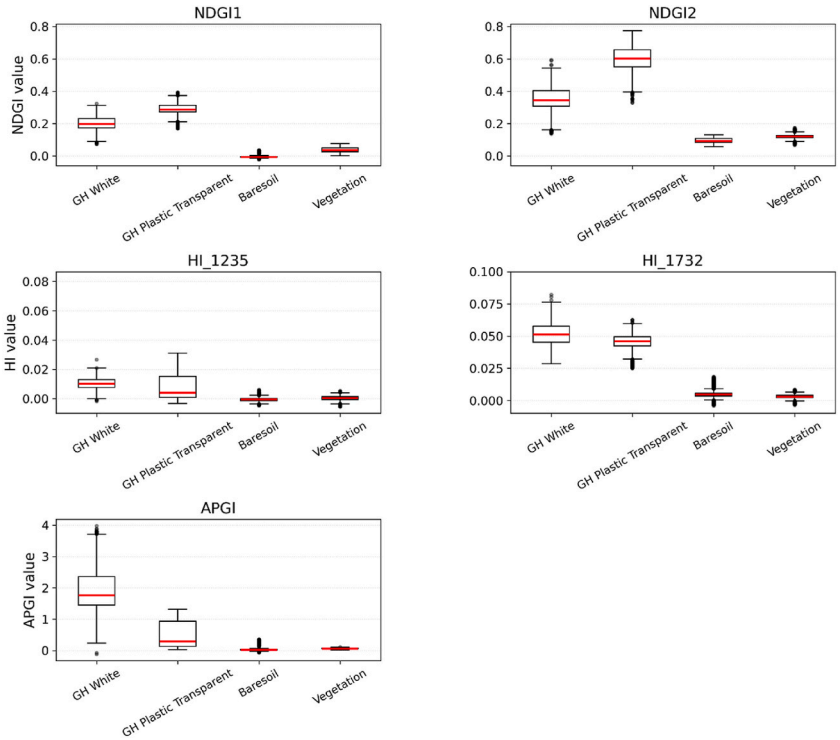

Fig. 7. Distribution of NDGI_1, NDGI_2, HI (1215 nm and 1732 nm formulations), and APGI values for the four land-cover classes (GH White, GH Plastic Transparent, Baresoil, and Vegetation) extracted from the AVIRIS-NG image. Boxplots show the median (horizontal line), interquartile range (boxes), and minimum–maximum range (whiskers).

3.3. Application of NDGI for plastic greenhouses mapping and accuracy

For mapping plastic greenhouses, $NDGI_1$ and $NDGI_2$ threshold values were fine-tuned to optimize the visual separation between greenhouse structures and other land covers. These threshold values were used to classify both the AVIRIS-NG image and the PRISMA-like image. By calculating and comparing the surface area occupied by greenhouses in the AVIRIS-NG and PRISMA-simulated images we assessed the consistency and robustness of the proposed indices across sensors with different spatial resolution and similar spectral characteristics.

The close-up view of a sub-area in the AVIRIS-NG image, together with the classification outputs obtained with the $NDGI_1$ and $NDGI_2$ indices, are shown in Fig. 6 (panels a, a.1, and a.2, respectively). The corresponding outputs from the PRISMA-like image simulated from AVIRIS-NG are shown in panels b, b.1, and b.2. In addition, panels c, c.1, and c.2 display the $NDGI_1$ and $NDGI_2$ classification results obtained from a real PRISMA image acquired over *Piana del Sele* on May 11, 2021, less than one month before the AVIRIS-NG flight occurred on June 03, 2021. Although the two acquisitions were not simultaneous, the greenhouse coverage and local conditions appeared comparable, allowing a consistent cross-sensor evaluation.

These images clearly showed the classification performance with high-spatial and -spectral resolution imagery. The additional analysis on the original PRISMA image confirmed the detectability of greenhouse structures at 30 m resolution, supporting the reliability of the $NDGI_1$ and $NDGI_2$ indices even when applied to spaceborne hyperspectral data acquired under different temporal conditions. For $NDGI_1$, a threshold value of 0.09 was found to be effective for delineating greenhouse areas. Using this threshold, the classification identified approximately 10.4 km^2 of greenhouses in the AVIRIS-NG image (detail in Fig. 6a1), 9.9 km^2 in the PRISMA-like image (close-up view in Fig. 6b1) and 10.12 km^2 in PRISMA original image (Fig. 6c1). For $NDGI_2$, a threshold of 0.20 was found. This resulted in the identification of 11.9 km^2 of greenhouses from AVIRIS-NG (detail in Fig. 6a2), 11.5 km^2 from PRISMA-like imagery (close-up view in Fig. 6b2) and 12.96 km^2 in PRISMA original image (Fig. 6c2). The total greenhouse area was computed by counting the number of pixels above the NDGI threshold and multiplying by the pixel area (2.7^2 m^2 for AVIRIS-NG and 30^2 m^2 for PRISMA-like and original PRISMA image). Both indices proved effective in detecting greenhouse structures, and no clear superiority was observed between them, although $NDGI_2$ appears to slightly overestimate greenhouse-covered areas, likely due to increased sensitivity to surrounding reflective surfaces. The choice between $NDGI_1$ and $NDGI_2$ may depend on the spectral bands available in the satellite imagery being used. For instance, hyperspectral sensors such as PRISMA, EnMAP, and DESIS provide coverage of both SWIR absorption regions, while multispectral instruments like WorldView-3 or Landsat-9 OLI include spectral bands overlapping with the $NDGI_2$ range (2200–2300 nm). Maintaining the two formulations separately therefore ensures flexibility and transferability, allowing $NDGI_1$ or $NDGI_2$ to be applied individually depending on the available sensor characteristics.

In the comparison between higher- and lower-spatial resolution (top versus bottom panels in Fig. 6), the classification results remained stable when the spatial resolution was reduced. This consistency across AVIRIS-NG, PRISMA-like, and original PRISMA data highlights the transferability of the NDGI-based approach to operational satellite missions. The comparison also highlights some limitations of the proposed indices. For instance, in the AVIRIS-NG classification with $NDGI_2$ (Fig. 6 panel a.2), certain linear features such as roads between greenhouses are partially misclassified as greenhouses. Similarly, in the PRISMA-like and original PRISMA classifications (Fig. 6 panels b.2 and c.2), small clusters of misclassified pixels can be observed in the top-right corner of the scene. These issues are likely related to mixed pixels and thresholding effects, which become more pronounced at coarser spatial resolutions and in heterogeneous areas. Despite these local misclassifications, the overall patterns remained consistent across the three datasets, supporting the robustness of the NDGI-based approach for mapping greenhouse structures.

Table 2
Summary statistics (minimum, maximum, mean, and standard deviation) of $NDGI_1$, $NDGI_2$, HI (1215 nm and 1732 nm formulations), and APGI values computed over the four ROI classes (GH White, GH Plastic Transparent, Baresoil, and Vegetation) in the AVIRIS-NG image.

Index	Class	Minimum	Maximum	Mean	Standard Deviation
$NDGI_1$	GH White	0.07	0.32	0.20	0.04
	GH Plastic Transparent	0.17	0.39	0.29	0.04
	Baresoil	−0.02	0.04	0.00	0.01
	Vegetation	0.00	0.08	0.04	0.02
$NDGI_2$	GH White	0.14	0.59	0.35	0.07
	GH Plastic Transparent	0.33	0.77	0.60	0.08
	Baresoil	0.06	0.13	0.10	0.02
	Vegetation	0.07	0.17	0.12	0.01
HI_1235	GH White	0.00	0.03	0.01	0.00
	GH Plastic Transparent	0.00	0.03	0.01	0.01
	Baresoil	0.00	0.01	0.00	0.00
	Vegetation	−0.01	0.01	0.00	0.00
HI_1732	GH White	0.03	0.08	0.05	0.01
	GH Plastic Transparent	0.02	0.06	0.05	0.01
	Baresoil	0.00	0.02	0.01	0.00
	Vegetation	0.00	0.01	0.00	0.00
APGI	GH White	−0.12	3.98	1.93	0.66
	GH Plastic Transparent	0.03	1.31	0.51	0.41
	Baresoil	−0.06	0.35	0.05	0.08
	Vegetation	0.01	0.11	0.06	0.02

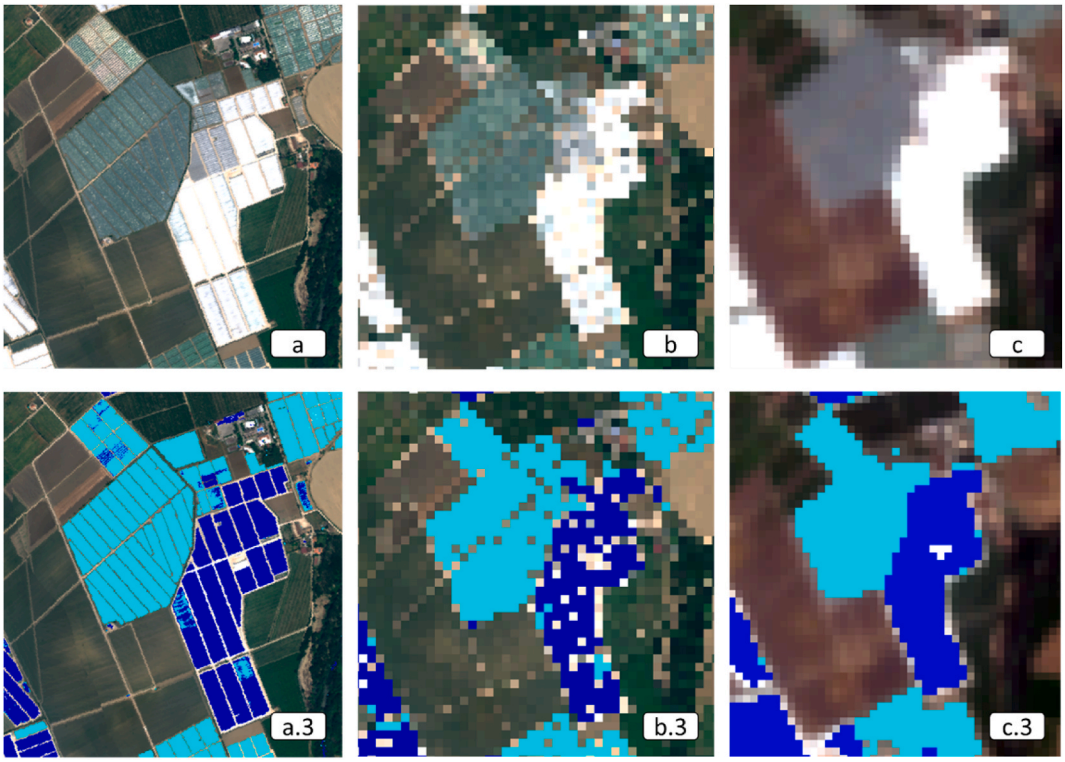

Fig. 8. Subsets of AVIRIS-NG (a, acquired on June 03, 2021), PRISMA-like (b, simulated from AVIRIS-NG), and real PRISMA image (c, acquired on May 11, 2021) over the Piana del Sele area. Panels a.3, b.3, and c.3 show the corresponding classification maps, where white (opaque) greenhouses are displayed in blue and transparent plastic greenhouses in cyan. Subset coordinates: ULC: WGS84 40.5909°N, 15.0160°E; LRC:40.5198°N, 15.0298°E.

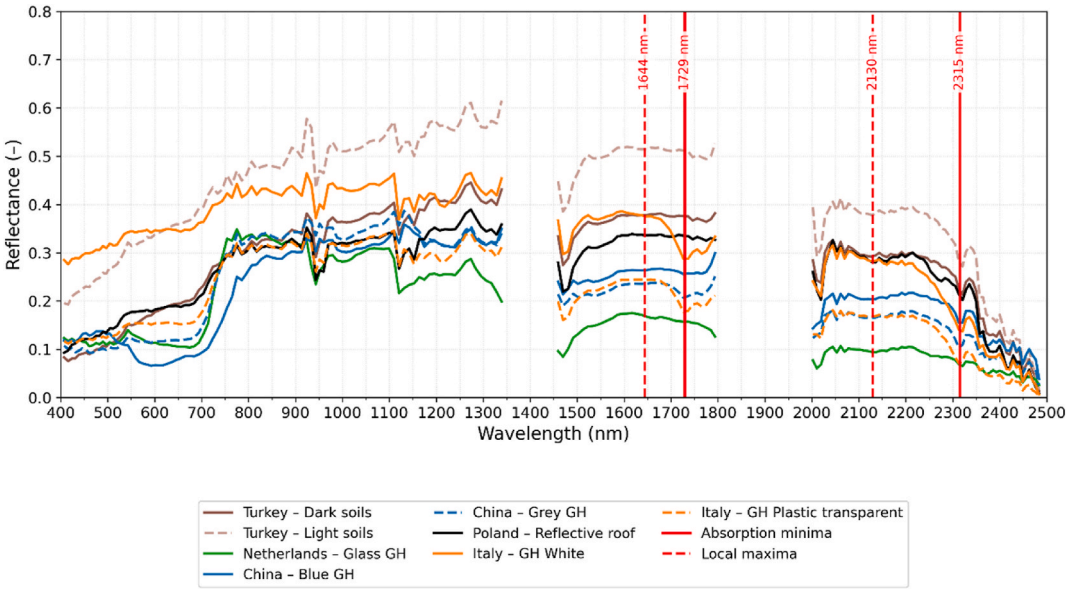

Fig. 9. Mean spectral signatures extracted from selected ROIs in the real PRISMA images, representing greenhouse structures and spectrally similar surfaces in five countries. The Italian ROIs (Piana del Sele, acquired on May 11, 2021) include white (opaque) and transparent plastic greenhouses ("Italy – GH White" and "Italy – GH Plastic Transparent"), while the other ROIs correspond to glass greenhouses (the Netherlands), plastic-covered greenhouses of different colours (China), light and dark soils (Turkey), and reflective roofs (Poland). Red solid and dashed vertical lines indicate the absorption minima and local maxima used for NDGI computation.

To assess the classification accuracy, we applied a confusion matrix using manually delineated ground-truth ROIs in the original AVIRIS-NG image selected from very high-resolution imagery and direct field surveys. The confusion matrix was used to compute the overall, producer's, and user's accuracy metrics for the AVIRIS-NG classification. The resulting accuracy for the greenhouse class reached 93.2 % for $NDGI_1$ and 89.9 % for $NDGI_2$, confirming the reliability of the classification results. No quantitative accuracy assessment was performed on PRISMA imagery, which was instead used to qualitatively test the transferability of the algorithm across sensors with largely different spatial resolutions.

We computed $NDGI_1$ and $NDGI_2$ values over the four ROI classes (GH White, GH Plastic Transparent, Baresoil, and Vegetation) within the AVIRIS-NG image to assess the separability between greenhouse and non-greenhouse surfaces. For comparison, we complemented the analysis with the APGI (Zhang et al., 2022) and the two versions of the HI (Kühn et al., 2004; Garaba and Dierssen, 2018) relative to the same ROIs (Fig. 7). $NDGI_1$ and $NDGI_2$ show the highest separability between greenhouse and other land covers, with narrow interquartile ranges within each class, indicating internal spectral homogeneity. The mean values of $NDGI_1$ range between 0.20 and 0.29 and those of $NDGI_2$ between 0.35 and 0.60 for greenhouses, while mean values are close to zero for bare soil and vegetation (Table 2). The high internal consistency across greenhouse pixels is quantified by the small standard deviations ranging between 0.04 and 0.08 (Table 2). The Hydrocarbon Index (HI) formulation centred on 1732 nm discriminate greenhouse surfaces effectively, with mean values of 0.05 for greenhouses and of about 0.00 for other land covers, whereas the HI 1215 nm formulation shows weaker contrast and higher within-class variability (Fig. 7 and Table 2). The APGI exhibits the largest spread of values, especially for white greenhouses (deviation standard of 0.66 around the mean of 1.93), and reduced separability from other land covers, consistent with its design for multispectral sensors lacking plastic-sensitive bands.

While both $NDGI_1$ and $NDGI_2$ effectively identify greenhouse structures, they do not allow for discrimination between different types of greenhouses, such as white (opaque) and transparent ones. Both types exhibit similar spectral responses in the SWIR region, which these indices primarily rely on, leading to their joint classification under the same category. To refine the classification, a third index commonly used in the scientific literature—the Normalized Difference Vegetation Index (NDVI)—can be effectively used (Jiang et al., 2006). When transparent plastic greenhouses cover active vegetation, the resulting spectral signature resembles that of green vegetation due to the strong reflectance in the near-infrared and absorption in the red wavelengths. By combining NDGI (for initial greenhouse detection) with NDVI (for type discrimination), it becomes possible to further classify the identified greenhouses. The

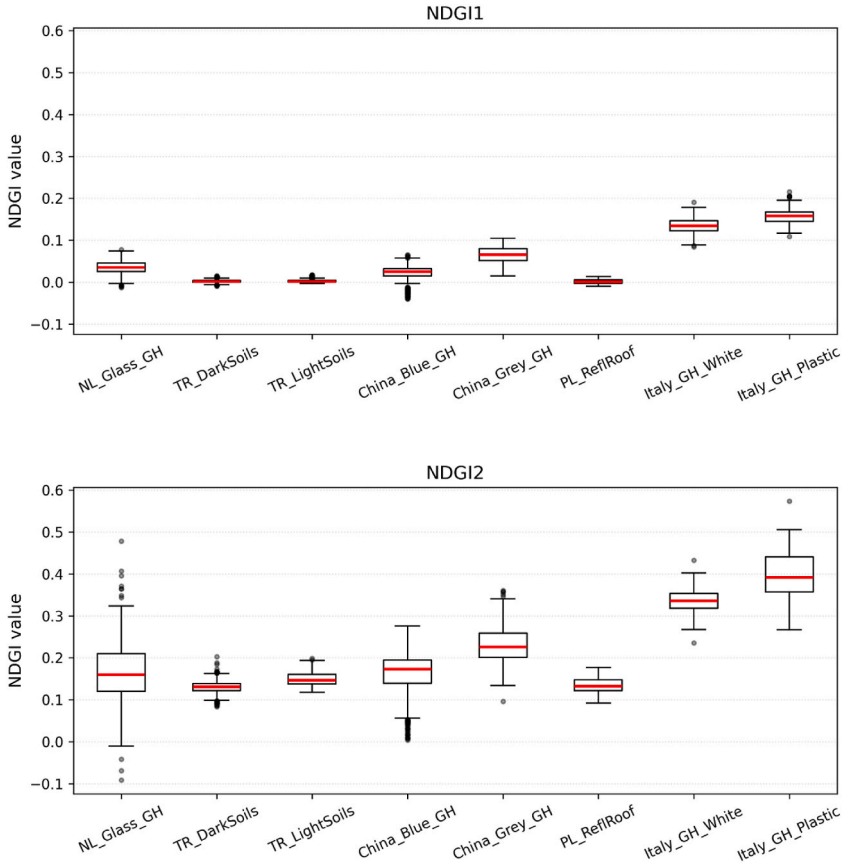

Fig. 10. Distribution of $NDGI_1$ and $NDGI_2$ values computed from PRISMA imagery over eight Regions of Interest (ROIs): NL_Glass_GH (the Netherlands), TR_DarkSoils and TR_LightSoils (Turkey), China_Blue_GH and China_Grey_GH (China), PL_ReflRoof (Poland), Italy_GH_White (Italy) and Italy_GH_Plastic (Italy). Boxplots show the median (red line), interquartile range (boxes), and full range (whiskers).

result is shown in Fig. 8 where the greenhouses previously detected using $NDGI_1$ were classified into two categories: white greenhouses and transparent plastic greenhouses. Using this approach, approximately 5.3 km^2 of white greenhouses and 5.1 km^2 of transparent plastic greenhouses were identified in the AVIRIS-NG image. The corresponding figures for the PRISMA-like image were 4.9 km^2 and 5.0 km^2, respectively. The distinction between white and transparent greenhouses in this study was confirmed through ground-truth information derived from visual interpretation of very high-resolution imagery, complemented by direct field surveys and in situ knowledge of the study area. These results confirm the feasibility of using NDGI in combination with NDVI to detect greenhouse structures and to provide preliminary insights into the optical properties of their plastic coverings (e.g., transparent versus opaque), depending on the extent to which vegetation signals are transmitted through the plastic.

In the classification maps of Fig. 8, some misclassifications are evident, particularly in panel (a.3), where portions of bare soil or non-greenhouse surfaces adjacent to greenhouse structures are incorrectly labelled as greenhouses. This effect is mainly due to the high reflectance similarity in the SWIR region between certain bright soil patches and plastic-covered roofs. In panel (b.3), the white spots correspond to pixels not assigned to either of the two greenhouse classes, which occur when spectral values fall close to the applied thresholds and do not meet the criteria for classification. Panel (c.3), derived from the original PRISMA image, shows a coarser delineation of greenhouse boundaries compared to AVIRIS-NG, with small greenhouse patches partially merged or fragmented due to the larger pixel size. These artifacts highlight the sensitivity of the method to mixed pixels and local spectral variability, which become more pronounced when moving from very high to coarser spatial resolution imagery.

3.4. Hyperspectral signatures retrieved from PRISMA imagery

The mean spectral signatures were calculated from PRISMA imagery for the land covers relevant in the context of plastic greenhouse mapping and are presented in Fig. 9.

Fig. 9 illustrates the distinct spectral behavior of greenhouse and non-greenhouse surfaces, particularly in the SWIR region where plastic absorption features are evident. The inclusion of the Italian ROIs (*Piana del Sele*, acquired on May 11, 2021) further highlights the characteristic absorption features of polyethylene-covered greenhouses. Both plastic greenhouses' spectra in Italy—representing white (opaque) and transparent plastic greenhouses—show clear minima at 1729 nm and 2315 nm, consistent with the plastic absorption features previously identified from AVIRIS-NG data.

For comparing the spectral shapes, we normalized the spectra to their maximum reflectance and computed pairwise Spectral Angle Mapper (SAM) distances (heatmap provided in the Supplementary Material). The SAM analysis highlights the partial separability of greenhouse covers from other land surfaces. Blue plastic greenhouses in China exhibit distinct spectral shapes compared to soils in Turkey, while grey plastic greenhouses show higher similarity with glass structures in the Netherlands. Reflective roofs in Poland, on the other hand, display strong spectral similarity with bare soils, whereas the Italian plastic greenhouses stand out as the most distinct class, confirming the diagnostic power of the SWIR absorption features.

To quantitatively evaluate this separability at satellite level, $NDGI_1$ and $NDGI_2$ values were computed over all ROIs extracted from PRISMA (Fig. 10). The calculated $NDGI_1$ and $NDGI_2$ values for the greenhouses in Italy are fully consistent with those derived from AVIRIS-NG, exceeding the thresholds defined for greenhouse detection ($NDGI_1 > 0.09$ and $NDGI_2 > 0.20$). Non-greenhouse surfaces display values below these limits, confirming the usefulness of the indices in reducing false positives, especially where high reflectance alone is not sufficient to confirm greenhouses presence. The result holds true also for greenhouses of atypical colours (blue rather than white/grey) located in China reflecting the ability of the indices to target the material properties. Overall, $NDGI_2$ appears slightly more robust than $NDGI_1$ in isolating greenhouse spectral features under PRISMA resolution, particularly in these selected challenging cases where other classifiers may fail or may need local calibration of the thresholds. However, the NDGI indices may yield weaker separability when the plastic-related minima are shallow or partly obscured by noise or atmospheric residuals following that the performance depends on the local spectral slope rather than the absolute absorption depth.

In this study, we focused on polyethylene (PE), the most commonly used material in the investigated areas. However, it is important to note that the most common greenhouse polymers share very similar absorption features in the SWIR region, particularly around 1730 and 2315 nm, which are well-documented in the literature (Castagna et al., 2023; Zhou et al., 2022). This spectral similarity suggests that the NDGI indices are not strongly dependent on the specific polymer type, but rather on the general presence of plastic covers. Further research is needed to comprehensively validate such result at other locations and over time. For completeness, the HI index at 1732 nm was also applied to the same PRISMA datasets (Fig. S1 in the Supplementary Material). The resulting boxplots confirm a comparable separability pattern to $NDGI_2$, with higher contrast for the "Chinese Grey GH" spectra where the absorption feature at 1729 nm is more pronounced.

4. Discussion

Our findings confirm that spectral resolution plays a crucial role in the identification of greenhouse structures, potentially prevailing over the influence of spatial resolution, which was tested here up to 30 m resolution to highlight the growing value of spaceborne hyperspectral missions for agricultural monitoring. This is consistent with prior studies (Jiménez-Lao et al., 2020; Kühn et al., 2004; Zhou et al., 2022), which identified diagnostic absorption features of plastic materials, particularly in the SWIR region, as essential for their detection. The diagnostic wavelengths selected for NDGI computation lie in the SWIR region, where polyethylene and other common greenhouse polymers (Zhou et al., 2022) exhibit well-known absorption features (minima at 1729 and 2315 nm, with adjacent maxima at 1644 and 2130 nm). These features provide strong separability from soils and vegetation, justifying the robustness of NDGI. However, the SWIR region is also partially affected by atmospheric water vapor absorption, and residual artifacts

from imperfect correction may attenuate these features under certain conditions, which need to be explored. Our results also demonstrate that $NDGI_1$ and $NDGI_2$ directly mitigate the misclassification issues often encountered with multispectral approaches, such as the OPAC algorithm. In particular, false positives over spectrally similar surfaces (soils or reflective roofs) were strongly reduced, highlighting the added value of hyperspectral data for reliable greenhouse mapping.

Similar to PRISMA, the EnMAP mission by DLR represents a hyperspectral demonstrator with acquisitions based on user requests or community tasking, while NASA's EMIT provides open-access hyperspectral data from the ISS. These missions, together with Planet's Tanager and the Kuva Space's Hyperfield-1, as well as forthcoming ones, such as ESA's PLATiNO-4 and CHIME missions, are expected to progressively overcome the limitations of current tasking-based acquisitions by offering higher acquisition frequencies and more systematic coverage. Such advances will enable routine use of hyperspectral data for global greenhouse mapping. In the context of multispectral missions, the Landsat Next satellites with instruments measuring 30 spectral bands will not allow for computing the NDGI with the current design. Adding narrow bands around the absorption features of $NDGI_1$ or $NDGI_2$ to future multispectral sensors would be highly advantageous for enabling continuous mapping of plastic-covered agricultural surfaces. Importantly, the NDGI-based classification was coherent over time in the tested *Piana del Sele*. The results confirmed the robustness of $NDGI_1$ and $NDGI_2$ under operational conditions and identified consistent classification patterns between airborne and spaceborne imagery. The comparative analysis between NDGI, HI, and APGI provides additional insights into the performance of the proposed indices. The NDGI indices demonstrated a high-fidelity discrimination between greenhouse and non-greenhouse surfaces. Their normalized two-band structure minimizes the influence of scene brightness and enhances transferability across sensors providing comparable SWIR coverage. $NDGI_2$, in particular, exhibited the highest class separability and the most stable responses across the analysed ROIs. The HI performed reasonably well in this study, particularly the formulation centred at 1732 nm, which effectively captured the characteristic SWIR absorption of greenhouse plastics. The HI indices showed lower overall dynamic ranges compared to $NDGI_1$ and $NDGI_2$. This behaviour is consistent with their linear (non-normalized) formulation, which makes them more sensitive to illumination, geometry, and reflectance magnitude. However, both HI formulations require three narrow and spectrally adjacent bands, a configuration well suited to hyperspectral sensors but less compatible with most multispectral instruments. The APGI, although designed for multispectral sensors such as Sentinel-2, exhibits limited separability between greenhouse and background classes in the hyperspectral domain, mainly due to its reliance on broad spectral bands and the need for location-specific thresholds. Looking ahead, the integration of multitemporal hyperspectral data could open up new possibilities for monitoring additional plastic-covered surfaces, such as agricultural mulch films of suitable spatial dimensions for satellite detection. Indeed, while OPAC could not distinguish plastic greenhouses and mulch using single images (la Cecilia et al., 2023), and it was therefore constrained to classify summer images to produce a pan-European map of greenhouses (la Cecilia and Despini, 2025), de Souza et al. (2024) resort to time-series analysis to identify plastic mulch. Moreover, future work should assess the potential of greenhouse detection approaches that are independent of excluding masks based on ancillary land cover datasets, allowing for more autonomous and scalable classification systems.

5. Conclusions

This study demonstrates the effectiveness of deriving simple hyperspectral remote sensing-based indices for mapping plastic greenhouses and distinguishing them from spectrally similar surfaces in agricultural landscapes using AVIRIS-NG data. The corresponding PRISMA analysis confirmed the transferability of the approach under spaceborne conditions, though with reduced separability due to coarser spatial resolution.

By analyzing high-resolution airborne AVIRIS-NG imagery, we identified key absorption features of plastic materials in the SWIR region, and we developed two normalized difference indices, $NDGI_1$ and $NDGI_2$. Both indices proved capable of detecting plastic greenhouses in the AVIRIS-NG data, with $NDGI_2$ showing slightly greater sensitivity.

The robustness of the indices was confirmed after a reduction in spatial resolution from 2.7 m (airborne sensor) to 30 m (spaceborne sensor). Importantly, both indices separated greenhouses from common false-positive classes such as bright soils and reflective roofs, indicating their suitability for operational use. It is important to note that the NDGI relies on relative reflectance contrasts (spectral slopes) between adjacent wavelengths, rather than on the absolute depth of absorption features. This formulation enhances transferability across sensors but may introduce sensitivity when the diagnostic minima are faint or partially masked.

The use of NDGI can be combined with NDVI to enable the discrimination between opaque (white) and transparent greenhouses, providing further insight into greenhouse typologies and potential crop conditions. This two-step approach offers a scalable solution for greenhouse monitoring, especially in areas where ground data is lacking. Also, a preliminary analysis pointed to temporal coherence of the NDGI thresholds for the same location.

This paper highlights the critical role of spectral resolution and wavelength bands selection in greenhouse detection and suggests that current and forthcoming hyperspectral missions will be key in supporting global, continuous, and accurate mapping of plastic-covered agricultural surfaces. Moreover, the identified spectral bands could guide the design of next-generation multispectral sensor. Future research should extend the validation of NDGI across the range of greenhouse types, geographical regions, and environmental conditions. In particular, its robustness under varying atmospheric conditions and different acquisition geometries should be assessed. The integration of multitemporal data, for instance through time-series analysis, could also further enhance greenhouse monitoring by capturing seasonal dynamics and reducing residual misclassifications.

CRediT authorship contribution statement

Francesca Despini: Writing – review & editing, Writing – original draft, Visualization, Investigation, Formal analysis, Data

curation. **Sofia Costanzini:** Writing – original draft, Writing – review & editing, Visualization, Investigation. **Davide Parmeggiani:** Writing – review & editing, Methodology, Formal analysis. **Daniele la Cecilia:** Writing – original draft, Writing – review & editing, Methodology, Data curation, Conceptualization.

Research data

The authors do not own the research data. These data can be freely downloaded from the following sources. AVIRIS-NG images are available at https://ares-observatory.ch/esa_chime_mission_2021/. PRISMA images are available upon registration at the link https://prismauserregistration.asi.it/. SCENE ID, Coordinates and ROIs are provided as Supplementary Materials.

Ethical statement

The authors declare that all ethical practices have been followed in relation to the development, writing and publication of the work reported in this paper.

Financial support

This research was complementary to the project REWATERING and received funding from the European Union's Horizon Europe research and innovation programme under the Marie Skłodowska-Curie grant agreement No. 101062255. The funding source was not involved from the research design to its dissemination.

Declaration of competing interest

The authors declare that they have no known competing financial interests or personal relationships that could have appeared to influence the work reported in this paper.

Acknowledgements

We acknowledge the two reviewers who provided excellent suggestions to improve the manuscript.

Appendix A. Supplementary data

Supplementary data to this article can be found online at https://doi.org/10.1016/j.rsase.2025.101802.

References

Acharki, S., Veettil, B.K., Vizzari, M., 2024. Plastic-covered greenhouses mapping in Morocco with Google Earth engine: comparing Sentinel-2 and Landsat-8 data using pixel-and object-based methods. Remote Sens. Appl.: Society and Environment 34, 101158.

Aguilar, M.Á., Jiménez-Lao, R., Nemmaoui, A., Aguilar, F.J., Koc-San, D., Tarantino, E., Chourak, M., 2020. Evaluation of the consistency of simultaneously acquired Sentinel-2 and Landsat 8 imagery on plastic covered greenhouses. Remote Sens. 12 (12), 2015.

Aguilar, M.A., Jiménez-Lao, R., Aguilar, F.J., 2021. Evaluation of object-based greenhouse mapping using WorldView-3 VNIR and SWIR data: a case study from Almeria (Spain). Remote Sens. 13 (11), 2133.

Ahemd, H.A., Al-Faraj, A.A., Abdel-Ghany, A.M., 2016. Shading greenhouses to improve the microclimate, energy and water saving in hot regions: a review. Sci. Hortic. 201, 36–45.

Aznar-Sánchez, J.A., Velasco-Muñoz, J.F., López-Felices, B., Román-Sánchez, I.M., 2020. An analysis of global research trends on greenhouse technology: towards a sustainable agriculture. Int. J. Environ. Res. Public Health 17, 664. https://doi.org/10.3390/ijerph17020664.

Briassoulis, D., 2023. Agricultural plastics as a potential threat to food security, health, and environment through soil pollution by microplastics: problem definition. Sci. Total Environ. 892, 164533.

Campra, P., Millstein, D., 2013. Mesoscale climatic simulation of surface air temperature cooling by highly reflective greenhouses in SE Spain. Environ. Sci. Technol. 47 (21), 12284–12290.

Castagna, A., Dierssen, H.M., Devriese, L.I., Everaert, G., Knaeps, E., Sterckx, S., 2023. Evaluation of historic and new detection algorithms for different types of plastics over land and water from hyperspectral data and imagery. Rem. Sens. Environ. 298, 113834.

Chapman, J.W., Thompson, D.R., Helmlinger, M.C., Bue, B.D., Green, R.O., Eastwood, M.L., et al., 2019. Spectral and radiometric calibration of the next generation airborne visible infrared spectrometer (AVIRIS-NG). Remote Sens. 11 (18), 2129.

Chen, L., Yu, L., Li, Y., Han, B., Zhang, J., Tao, S., Liu, W., 2022. Spatial distributions, compositional profiles, potential sources, and influencing factors of microplastics in soils from different agricultural farmlands in China: a national perspective. Environ. Sci. Technol. 56 (23), 16964–16974.

Cogliati, S., Sarti, F., Chiarantini, L., Cosi, M., Lorusso, R., Lopinto, E., et al., 2021. The PRISMA imaging spectroscopy mission: overview and first performance analysis. Rem. Sens. Environ. 262, 112499.

De Gelder, A., Poot, E.H., Dieleman, J.A., De Zwart, H.F., 2011. A concept for reduced energy demand of greenhouses: the next generation greenhouse cultivation in the Netherlands. International Symposium on Advanced Technologies and Management Towards Sustainable Greenhouse Ecosystems: Greensys2011 952, pp. 539–544.

De Luca, G., Pancorbo, J.L., Carotenuto, F., Gioli, B., Modica, G., Genesio, L., 2025. PRISMA imaging for land covers and surface materials composition in urban and rural areas adopting multiple endmember spectral mixture analysis (MESMA). ISPRS J. Photogrammetry Remote Sens. 225, 196–220.

de Souza, M.F., Lamparelli, R.A., Oliveira, M.H., Nogueira, G.P., Bliska Jr, A., Franco, T.T., 2024. Remote sensing detection of plastic-mulched farmland using a temporal approach in machine learning: case study in tomato crops. Environ. Sci. Pollut. Control Ser. 1–14.

Espí, E., Salmerón, A., Fontecha, A., García, Y., Real, A.I., 2006. Plastic films for agricultural applications. J. Plast. Film Sheeting 22 (2), 85–102.
Estrela, R., Thompson, D.R., Brodrick, P.G., Chadwick, K.D., Gierach, M.M., Luis, K., et al., 2024. Worldwide Detection of Plastic from Space with the EMIT Imaging Spectrometer. Authorea Preprints.
Freitas, S., Silva, H., Silva, E., 2021. Remote hyperspectral imaging acquisition and characterization for marine litter detection. Remote Sens. 13 (13), 2536.
Garaba, S.P., Dierssen, H.M., 2018. An airborne remote sensing case study of synthetic hydrocarbon detection using short wave infrared absorption features identified from marine-harvested macro-and microplastics. Rem. Sens. Environ. 205, 224–235.
Gerritsen, A.L., Groot, A.M.E., Nieuwenhuizen, W., 2014. Glasshouse Horticulture in the Netherlands: Governance for Resilient and Sustainable Economies, pp. 1–24. Alterra.
Giacomelli, G.A., Roberts, W.J., 1993. Greenhouse covering systems. HortTechnology 3 (1), 50–58.
Green, R.O., Eastwood, M.L., Sarture, C.M., Chrien, T.G., Aronsson, M., Chippendale, B.J., et al., 1998. Imaging spectroscopy and the airborne visible/infrared imaging spectrometer (AVIRIS). Rem. Sens. Environ. 65 (3), 227–248.
Green, R.O., Brodrick, P.G., Chapman, J.W., Eastwood, M., Geier, S., Helmlinger, M., et al., 2023. AVIRIS-NG L2 Surface Reflectance, Facility Instrument Collection, V1. ORNL DAAC, Oak Ridge, Tennessee, USA.
Guo, J.J., Huang, X.P., Xiang, L., Wang, Y.Z., Li, Y.W., Li, H., et al., 2020. Source, migration and toxicology of microplastics in soil. Environ. Int. 137, 105263.
Hati, J.P., Samanta, S., Chaube, N.R., Misra, A., Giri, S., Pramanick, N., et al., 2021. Mangrove classification using airborne hyperspectral AVIRIS-NG and comparing with other spaceborne hyperspectral and multispectral data. The Egyptian Journal of Remote Sensing and Space Science 24 (2), 273–281.
Hsieh, P.F., Lee, L.C., Chen, N.Y., 2001. Effect of spatial resolution on classification errors of pure and mixed pixels in remote sensing. IEEE Trans. Geosci. Rem. Sens. 39 (12), 2657–2663.
Hu, J., Gettel, G., Fan, Z., Lv, H., Zhao, Y., Yu, Y., et al., 2021. Drip fertigation promotes water and nitrogen use efficiency and yield stability through improved root growth for tomatoes in plastic greenhouse production. Agric. Ecosyst. Environ. 313, 107379.
Huang, Y., Liu, Q., Jia, W., Yan, C., Wang, J., 2020. Agricultural plastic mulching as a source of microplastics in the terrestrial environment. Environ. Pollut. 260, 114096.
Hussain, I., Hamid, H., 2003. Plastics in agriculture. Plastics and the Environment. Wiley, Hoboken, pp. 185–209.
Jiang, Z., Huete, A.R., Chen, J., Chen, Y., Li, J., Yan, G., Zhang, X., 2006. Analysis of NDVI and scaled difference vegetation index retrievals of vegetation fraction. Rem. Sens. Environ. 101 (3), 366–378.
Jiménez-Lao, R., Aguilar, F.J., Nemmaoui, A., Aguilar, M.A., 2020. Remote sensing of agricultural greenhouses and plastic-mulched farmland: an analysis of worldwide research. Remote Sens. 12 (16), 2649.
Jiménez-Lao, R., Aguilar, M.A., Aguilar, F.J., 2022. Plastic cover greenhouses reflectance spectra from different optical satellite imagery. Int. Arch. Photogram. Rem. Sens. Spatial Inf. Sci. 43, 585–592.
Kendirli, B., 2006. Structural analysis of greenhouses: a case study in Turkey. Build. Environ. 41 (7), 864–871.
Kühn, F., Oppermann, K., Hörig, B., 2004. Hydrocarbon Index – an algorithm for hyperspectral detection of hydrocarbons. Int. J. Rem. Sens. 25 (12), 2467–2473.
Kuśmierski, J., Hodor, K., 2024. Historical orangeries and greenhouses in Poland: typology and preservation. Architectus.
la Cecilia, D., Tom, M., Stamm, C., Odermatt, D., 2023. Pixel-based mapping of open field and protected agriculture using constrained Sentinel-2 data. ISPRS Open Journal of Photogrammetry and Remote Sensing 8, 100033.
la Cecilia, D., Philipp, M., Kaegi, R., Schirmer, M., Moeck, C., 2024. Microplastics attenuation from surface water to drinking water: impact of treatment and managed aquifer recharge–and identification uncertainties. Sci. Total Environ. 908, 168378.
la Cecilia, D., Venezia, A., Massa, D., Camporese, M., 2025. From weather data to water fluxes simulation in Mediterranean greenhouses through a combined climate and hydrological modelling approach. Agric. Water Manag. 311, 109386.
la Cecilia, D., Despini, F., 2025. Protected agriculture mapping at continental scale for highlighting hotspots of altered hydrological processes. Remote Sens. Appl.: Society and Environment 37, 101509.
Lanorte, A., De Santis, F., Nolè, G., Blanco, I., Loisi, R.V., Schettini, E., Vox, G., 2017. Agricultural plastic waste spatial estimation by Landsat 8 satellite images. Comput. Electron. Agric. 141, 35–45.
Lehel, J., Murphy, S., 2021. Microplastics in the food chain: food safety and environmental aspects. Rev. Environ. Contam. Toxicol. 259, 1–49.
Levin, N., Lugassi, R., Ramon, U., Braun, O., Ben-Dor, E., 2007. Remote sensing as a tool for monitoring plasticulture in agricultural landscapes. Int. J. Rem. Sens. 28 (1), 183–202.
Liu, X., Xin, L., 2023. Spatial and temporal evolution and greenhouse gas emissions of China's agricultural plastic greenhouses. Sci. Total Environ. 863, 160810.
Liu, Y.N., Sun, D.X., Hu, X.N., Ye, X., Li, Y.D., Liu, S.F., et al., 2019. The advanced hyperspectral imager: aboard China's GaoFen-5 satellite. IEEE Geoscience and Remote Sensing Magazine 7 (4), 23–32.
Loizzo, R., Guarini, R., Longo, F., Scopa, T., Formaro, R., Facchinetti, C., Varacalli, G., 2018. PRISMA: the Italian hyperspectral mission. In: IGARSS 2018-2018 IEEE International Geoscience and Remote Sensing Symposium. IEEE, pp. 175–178.
McCullum, A., Torres-Pérez, J., Bengtsson, Z., 2021. Hyperspectral data for land and coastal systems. NASA Applied Remote Sensing Training Program (ARSET). https://appliedsciences.nasa.gov/join-mission/training/english/arset-hyperspectral-data-land-and-coastal-systems.
Picariello, E., Fornasier, F., Bilotto, M., Mignoli, E., Baiano, S., Morra, L., 2024. Eco-sustainability of soils in baby-leaf crop systems under tunnel through the application of c-rich inputs: towards combating soil degradation. Horticulturae 10 (5), 476.
Pignatti, S., Palombo, A., Pascucci, S., Romano, F., Santini, F., Simoniello, T., et al., 2013. The PRISMA hyperspectral mission: science activities and opportunities for agriculture and land monitoring. In: 2013 IEEE International Geoscience and Remote Sensing symposium-IGARSS. IEEE, pp. 4558–4561.
Qi, R., Tang, Y., Jones, D.L., He, W., Yan, C., 2023. Occurrence and characteristics of microplastics in soils from greenhouse and open-field cultivation using plastic mulch film. Sci. Total Environ. 905, 166935.
Robson, T.M., Pieristè, M., Durand, M., Kotilainen, T.K., Aphalo, P.J., 2022. The benefits of informed management of sunlight in production greenhouses and polytunnels. Plants, People, Planet 4 (4), 314–325.
Savic, D., Ilin, Z.M., 2022. Advantages of growing vegetable crops in modern greenhouses. In: Vegetable Crops-Health Benefits and Cultivation. IntechOpen.
Scarascia-Mugnozza, G., Sica, C., Russo, G., 2011. Plastic materials in European agriculture: actual use and perspectives. J. Agric. Eng. 42 (3), 15–28.
Shi, L., Huang, X., Zhong, T., Taubenböck, H., 2019. Mapping plastic greenhouses using spectral metrics derived from GaoFen-2 satellite data. IEEE J. Sel. Top. Appl. Earth Obs. Rem. Sens. 13, 49–59.
Tang, K.H.D., 2023. Microplastics in agricultural soils in China: sources, impacts and solutions. Environ. Pollut. 322, 121235.
Thompson, D.R., Gao, B.C., Green, R.O., Roberts, D.A., Dennison, P.E., Lundeen, S.R., 2015. Atmospheric correction for global mapping spectroscopy: ATREM advances for the HyspIRI preparatory campaign. Rem. Sens. Environ. 167, 64–77.
Thorpe, A.K., Frankenberg, C., Aubrey, A.D., Roberts, D.A., Nottrott, A.A., Rahn, T.A., et al., 2016. Mapping methane concentrations from a controlled release experiment using the next generation airborne visible/infrared imaging spectrometer (AVIRIS-NG). Rem. Sens. Environ. 179, 104–115.
Tong, X., Zhang, X., Fensholt, R., Jensen, P.R.D., Li, S., Larsen, M.N., et al., 2024. Global area boom for greenhouse cultivation revealed by satellite mapping. Nat. Food 5 (6), 513–523.
Vali, A., Comai, S., Matteucci, M., 2020. Deep learning for land use and land cover classification based on hyperspectral and multispectral Earth observation data: a review. Remote Sens. 12 (15), 2495.
Veettil, B.K., Van, D.D., Quang, N.X., Hoai, P.N., 2023. Remote sensing of plastic-covered greenhouses and plastic-mulched farmlands: current trends and future perspectives. Land Degrad. Dev. 34 (3), 591–609.
Wang, J., Lv, S., Zhang, M., Chen, G., Zhu, T., Zhang, S., et al., 2016. Effects of plastic film residues on occurrence of phthalates and microbial activity in soils. Chemosphere 151, 171–177.
Wang, K., Chen, W., Tian, J., Niu, F., Xing, Y., Wu, Y., et al., 2022. Accumulation of microplastics in greenhouse soil after long-term plastic film mulching in Beijing, China. Sci. Total Environ. 828, 154544.

Wittwer, S.H., 1993. World-wide use of plastics in horticultural production. HortTechnology 3 (1), 6–19.
Yang, D., Chen, J., Zhou, Y., Chen, X., Chen, X., Cao, X., 2017. Mapping plastic greenhouse with medium spatial resolution satellite data: development of a new spectral index. ISPRS J. Photogrammetry Remote Sens. 128, 47–60.
Zhang, P., Du, P., Guo, S., Zhang, W., Tang, P., Chen, J., Zheng, H., 2022. A novel index for robust and large-scale mapping of plastic greenhouse from Sentinel-2 images. Rem. Sens. Environ. 276, 113042.
Zhou, S., Kaufmann, H., Bohn, N., Bochow, M., Kuester, T., Segl, K., 2022. Identifying distinct plastics in hyperspectral experimental lab-, aircraft-, and satellite data using machine/deep learning methods trained with synthetically mixed spectral data. Rem. Sens. Environ. 281, 113263.